Desalination and Water Treatment
www.deswater.com
doi: 10.5004/dwt.2019.23704

147 (2019) 255–263
April

Synthesis of novel biochar substrate from harvested *Cyperus alternifolius* and its applicable potential for fluoride removal from river waters in artificial floating beds

Chaoguang Gu[a,b], Shuang Song[a,b], Shuyi Chu[c], Jibo Xiao[d,*], Ronald W Thring[d,e], Lingzhou Cui[d]

[a]*College of Environment, Zhejiang University of Technology, Hangzhou 310014, China*
[b]*Collaborative Innovation Center of Yangtze River Delta Region Green Pharmaceuticals, Zhejiang University of Technology, Hangzhou 310014, China*
[c]*Wenzhou Vocational College of Science and Technology, Wenzhou 325000, China*
[d]*College of Life and Environmental Science, Wenzhou University, Wenzhou 325035, China, email: jbxiao@126.com (J. Xiao)*
[e]*Environmental Science and Engineering, University of Northern British Columbia, Prince George, British Columbia, Canada*

Received 18 April 2018; Accepted 31 December 2018

ABSTRACT

Fe-impregnated biochar (FeBC) substrates were prepared from harvested *Cyperus alternifolius* at pyrolysis temperatures of 400°C, 600°C, and 800°C. Surfaces of obtained biochars were characterized by scanning electron micrograph, Brunauer-Emmett-Teller, and Fourier transform infrared spectroscopy. The performance of FeBC to remove fluoride from aqueous solution was investigated under varying conditions of pH, adsorbent dosage, and contact time. The potential of fluoride removal from polluted waters in artificial floating beds with FeBC as substrates was studied. The results showed that fluoride removal was not affected significantly by the variation of pH and remained above 90% over the entire pH range of 2.0–10.0. The pseudo-second-order model was found to best describe the adsorption kinetics. The maximum adsorption capacity values were 13.624, 14.144, and 14.706 mg g^{-1} under temperatures of 293, 303, and 313 K, respectively. The artificial floating beds with FeBC-rooted *Cyperus alternifolius* could remove 81.6% F at day 10 for initial fluoride concentration of 5 mg L^{-1}. Thus, FeBC may be a feasible alternative in the removal of fluoride from contaminated waters.

Keywords: Fluoride; Biochar; Fe-impregnated; Substrate; Adsorption; Artificial floating bed

1. Introduction

Fluorine is an extremely reactive nonmetallic element that is widely used in industries such as aluminum smelters, stainless steel, brick, ceramics, pharmaceutical, semiconductor, and electroplating [1]. Fluoride concentrations in groundwater much higher than the maximum permissible limit have been found in many regions throughout the world [2–4]. Recently in China, fluoride has been detected in surface waters at concentrations that exceed the country's water quality criteria. For example, average fluoride concentrations in the Lunchuan and Zhongheng rivers in Wenzhou City, Zhejiang Province, were reported as 4.73 and 3.80 mg L^{-1} in 2014 according to the data from environmental monitoring agents. The elevated fluoride was attributed to the direct discharge of effluents from nearby stainless steel and electroplating industries. Fluorine is an essential element for humans and animals. Epidemiological evidence suggests that fluorine has a beneficial effect on bone formation in both humans and animals, and it certainly appears to inhibit osteoporosis [1]. However, an excess uptake of fluorine leads to fluorosis of teeth and bones and induces neurological damage, kidney diseases, brain damage, cancer, and thyroid disorders [5].

* Corresponding author.

Aquatic plants were serendipitously found to be able to absorb the fluoride from contaminated waters in the Lunchuan river during a remediation project conducted in 2015 to reduce nitrogen and phosphorus. The average fluoride concentration decreased to about 2.36 mg L^{-1}. Several aquatic plants have been reported to be capable of accumulating F in their tissues [6–8]. For example, milfoil (*Myriophyllum spicatum* L.) and hornwort (*Ceratophyllum demersum* L.) in an F-polluted water reservoir bioconcentrated 778 and 1,060 mg F kg^{-1} dry mass, respectively [9]. Another study on reeds revealed that F levels in the roots, stalks, and leaves from such plants in an F-polluted reservoir were as high as 213, 36.8, and 51.5 mg F kg^{-1} dry mass, respectively [10]. However, the fluoride concentration in the Lunchuan river water could not be reduced below the permissible limit. Thus, other technologies are urgently needed to further reduce the fluoride levels.

Conventional methods available for the removal of fluoride from aqueous solution include chemical precipitation [11], adsorption [12], ion exchange [13], coagulation [14], and reverse osmosis [15]. Among these technologies, chemical precipitation and coagulation are very common to reduce high concentrations of fluoride from industrial wastewaters (fluoride concentration ≥ 100mg L^{-1}). Reverse osmosis and ion exchange are effective in removing fluoride to the desired levels; however, they are not used on a large scale due to high installation and operation costs, as well as increased complexity in the processes [5]. Adsorption has been proven to be the simplest and the most efficient method of separation, especially for removing low concentrations of pollutants [16–20]. Thus, combination of adsorption process of adsorbent and absorption of macrophyte may be a feasible alternative to reduce fluoride concentrations in polluted waters to permissible levels. Since the adsorption capacity of conventional adsorbent was relatively limited, many researchers focused on the modification of natural adsorbent, for example, impregnation of metal compounds [21], such as iron(III) and aluminum(III), the use of microwave radiation [22], the preparation of nanostructured adsorbent [23–27], etc.

Biochar is a carbonaceous material obtained from thermal decomposition of biomass with little or no oxygen [28]. It is known as an amendment to improve the physicochemical and biological properties of soils to enhance plant growth [29]. Many studies have also shown that biochar is a promising low-cost adsorbent in the removal of organic pollutants, heavy metals, and phosphorus from waters [30]. However, reports on adsorption of fluoride on biochar are still relatively limited [31]. The properties of biochar depend on feedstock characteristics and pyrolysis conditions, and the pyrolysis temperature is a key factor with a great impact on specific surface area and surface functional groups on biochar [30].

Cyperus alternifolius is a rhizomatous, herbaceous, perennial, and emergent macrophyte with stems 100–250 cm in length. Due to the large root surface areas, it is widely used for phytoremediation of polluted waters [32,33]. However, the plant biomass above the water surface has to be removed periodically from the waters to maintain remediation efficiency [34]. Furthermore, the plant withers away and goes into dormancy in winter when the temperature is 4°C or lower. If the plant biomass is not harvested, the nutrients that have been incorporated into the plant tissues would be returned to the waters during the decaying process [35]. Hence, a large amount of biomass residues is generated annually. Recently, most of them are disposed in landfills as domestic solid wastes, which does not only increase the landfill load significantly but also results in a great waste of resources. Over 85% of the above-ground biomass is stem that consists primarily of high-density vascular bundle tissues [36], indicating it may be a suitable precursor for adsorbent production.

The objectives of the present work are to (1) synthesize biochar substrate with high adsorption capacity for fluoride from harvested *Cyperus alternifolius*, (2) explore the potential of artificial floating beds with the obtained biochar as a substrate in removing fluoride from waters, (3) reveal the influence of pyrolysis temperature on structural, morphological, and adsorption properties of the produced biochar, (4) investigate the effects of pH, adsorbent dosage, and contact time on fluoride removal, and (5) analyze the kinetic data using different mathematical models.

2. Materials and methods

2.1. Raw materials

Cyperus alternifolius was collected from a small pond at the Zhejiang Agriculture and Forestry University in November 2015. All chemicals (sodium fluoride, ferric chloride, potassium nitrate, hydrochloric acid, sodium hydroxide) used in this study were of analytical grade, and the solutions were prepared with distilled water. A stock solution of 2,100 mg L^{-1} was prepared by dissolving 2.1000 g sodium fluoride in 1,000 mL distilled water. The experimental solution was prepared by diluting the stock solution with distilled water as needed.

2.2. Synthesis of biochars with Cyperus alternifolius

Cyperus alternifolius was carefully washed with tap water, air-dried, and ground up using a crusher machine to a length of 2–5 mm. The ground *Cyperus alternifolius* was then soaked thoroughly in ferric chloride solution (1.0 mol L^{-1}) at a CA:$FeCl_3$ mass ratio of 1:15 for 24 h. The Fe-impregnated biomass was then separated from the solution and pyrolyzed in a muffle furnace. The temperature was ramped up from ambient to a final temperature of 600°C with a retention time of 2 h. The resultant biochar, identified as BFeC600, was washed with distilled water several times and then dried at 105°C in the oven for 12 h.

Fe-impregnated biochar (FeBC) was prepared as follows: the ground *Cyperus alternifolius* was pyrolyzed at the final temperature of 400°C, 600°C, and 800°C with a retention time of 2 h, respectively. The obtained biochars were subsequently impregnated with ferric chloride (1.0 mol L^{-1}) at a mass ratio of 1:15 for 24 h. The FeBCs, identified as FeBC400, FeBC600, and FeBC800, were all washed with distilled water several times and then dried at 105°C in the oven for 12 h.

2.3. Characterization of adsorbents

The specific surface area and pore structure were measured using an accelerated surface area and porosimetry

system (USA, Micromeritics ASAP 2020) using N_2 gas as adsorbate at 77.37 K. The micropore area and micropore volume were determined by the *t*-plot. A Hitachi S4700 series scanning electron microscope (SEM) was used to observe the surface physical morphology of adsorbents. The surface groups on the adsorbents were identified by Fourier transform infrared (FTIR) spectroscopy using the KBr disk technique. The transmission FTIR spectrum was recorded between 400 and 4,000 cm^{-1} using a Nicolet 6700 series FTIR spectrometer.

2.4. Adsorption experiments

A fixed amount of adsorbent was added into 250-mL conical flasks containing 100 mL sodium fluoride solution. The pH of the solution was adjusted using 0.1 M NaOH and 0.1 M HCl solutions before addition of adsorbent. The flasks were then placed in a thermostated shaker at 130 rpm for 2 h at 20°C. The adsorbent was removed from the aqueous solution, and the filtrates were then analyzed for the residual fluoride concentration by fluoride ion-selective electrode (PXS-450, China). Adsorption kinetics were carried out with fluoride concentrations of 10 and 30 mg L^{-1} at 1, 2, 5, 10, 15, 20, 30, 60, 90, and 180 min. Adsorption isotherm studies were carried out with six different initial concentrations of fluoride from 5 to 200 mg L^{-1} at temperatures of 293, 303, and 313 K. The experiments were conducted in triplicate.

2.5. Fluoride removal in artificial floating beds with FeBC as substrates

The trial was conducted in six separate rectangular plastic tanks (0.65 m length × 0.5 m width × 0.35 m height) with a working depth of 0.3 m. High-density polyethylene foam plates were used to provide the necessary buoyancy in the ecological floating systems (Fig. 1). *Cyperus alternifolius* samples were collected and rinsed to remove mud, debris, and invertebrate grazers before pre-culturing for 2 weeks. The sturdy plants (approximately 25–30 cm in length) were transplanted into the culture buckets. Each bucket was planted with two *Cyperus alternifolius*. The experimental bucket was filled with 310.50 g FeBC600 (dry weight), which was mixed with deionized water before being planted in the bucket. The plants in the control buckets were winded with sponge. Initial fluoride concentration was 5 mg L^{-1}, and pH was not adjusted. The trial was conducted under natural light and a water temperature of 30.2°C–31.5°C. Losses in water volume due to evapotranspiration were compensated by the addition of deionized water every other day to maintain the original level. Both the experiment and control groups were performed in triplicate.

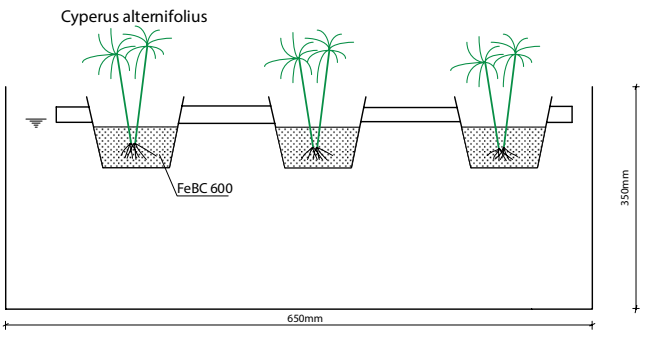

Fig. 1. Schematic diagram of artificial floating bed system.

2.6. Desorption and regeneration of FeBC

Desorption of FeBC was carried out using 1.0 mol L^{-1} HCl solution, followed by water rinsing till pH of washing reached around 7. The FeBC was then immersed thoroughly in ferric chloride solution (1.0 mol L^{-1}) at a mass ratio of 1:15 for 24 h to be regenerated for fluoride adsorption again. After each experiment, the solutions were filtered and the filtrates were then analyzed for the residual fluoride concentration.

3. Results and discussion

3.1. Fluoride removal by adsorbents derived from Cyperus alternifolius

Different adsorbents derived from *Cyperus alternifolius* were used to remove fluoride from aqueous solution (Fig. 2). It can be seen that the percentage of fluoride removal on the Fe-impregnated *Cyperus alternifolius* (FeC) is much higher than from the raw sample. The high adsorption capacity of FeC is probably due to the changes of both physical and chemical characteristics of *Cyperus alternifolius*. Fe-impregnated biomass has been reported to have a rough surface morphology and higher Brunauer-Emmett-Teller surface area [37]. Additionally, the electrostatic interaction between positively charged ion compounds and negatively charged fluoride ions significantly enhanced the adsorption.

Inorganic salts could also significantly accelerate the degradation of hemicellulose [38] and increase the micropore volume and specific surface area of biomass-derived biochar obtained [39]. However, some researchers have

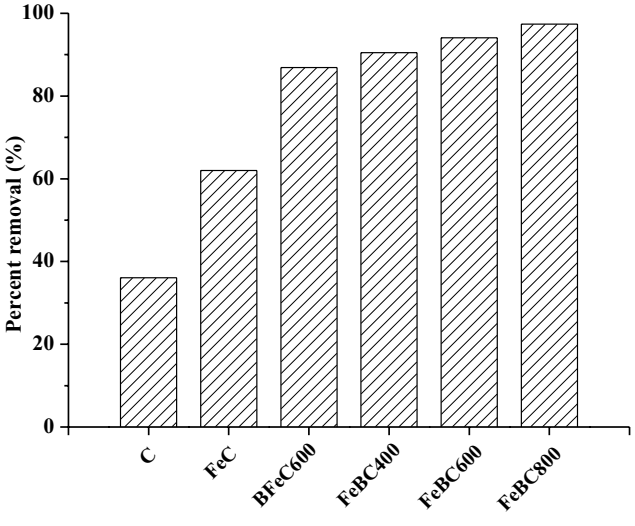

Fig. 2. Fluoride removal by different adsorbents derived from *Cyperus alternifolius*.

reported that the biochar has lower surface area, especially when salts are impregnated at higher concentration [40]. It is speculated that salts catalyzed the char-forming secondary reactions by promoting volatile condensation, which is known to block the pores [41]. The average pore radius is larger owing to the redox reaction of iron oxides and carbon wall [42]. Liu et al. [43] observed that modification of activated carbon by Fe(III) enlarged pore size, reduce pore volume and specific surface, but enhance the formation of effective surface functional groups. As shown in Fig. 2, the removal of fluoride by FeBC600 is 8.2% higher than BFeC600, indicating that functional groups enhance the adsorption process. Furthermore, fluoride removal by FeBC increased with increasing pyrolysis temperature. Such adsorption features are also reported on other biochars for benzene [44], naphthalene [45], and catechol [46]. This might be attributed to the development of porous structures on biochar with increasing pyrolysis temperature [47].

3.2. Textural morphological characteristics of FeBC

Fig. 3 shows the SEM photographs of FeBC400, FeBC600, and FeBC800. The vertical cross sections of the three biochars are relatively smooth except for a few small grooves and cracks, whereas the horizontal cross sections are quite irregular and filled with pores of different sizes and shapes. The porous structure of the biochars developed gradually with pyrolysis temperature. As shown in Table 1, FeBC800 displays the highest BET surface area (429.72 $m^2 g^{-1}$) and pore volume (0.30 $m^3 g^{-1}$). This is consistent with the observations reported by Brown et al. [48]. The increase of surface area and pore volume might be attributed to the pyrolysis behavior of chemical components within biomass. Hemicellulose decomposed at 220°C–315°C and cellulose at 315°C–400°C [49]. The lignin, comprised of aromatic rings joined by –C–C– and –C–O–C– covalent bonds, was the most difficult to decompose, occurring within a wide temperature range of 100°C–900°C [49].

Nitrogen adsorption/desorption isotherms and pore size distributions for FeBC400, FeBC600, and FeBC800 are depicted in Fig. 4. According to the International Union of Pure and Applied Chemistry (IUPAC) nomenclature, such isotherms are of the IV type with hysteresis loop, which suggests the existence of mesopores in these adsorbents due to capillary condensation within the pores. The distinct hysteresis loop indicates slit-shaped pores where the adsorption and desorption branches are parallel [50]. As seen, all the pore size distribution curves in $dV/d\log$ have a peak at a diameter less than 2 nm, indicating the presence of micropore structures. The percentages of micropore surface area of the three biochars are determined to be 85.54%, 83.94%, and 81.98%, respectively. It should be noticed that the percentage of micropore volume of FeBC600 is greater than FeBC800; yet, the average pore diameter of FeBC600 is 2.66 nm, which is the smallest of the three biochar samples. Bonelli et al. [51] also reported that structural ordering, pore widening, or the coalescence of neighboring pores may occur at higher temperature (850°C), leading to a decrease in micropore volume.

3.3. Surface functional groups on FeBC

The FTIR spectra of FeBC obtained at different pyrolysis temperatures are presented in Fig. 5. The intensity of peaks at 1,570, 1,120, 840, and 480 cm^{-1} all increased with increasing pyrolysis temperature. The band observed at 1,570 cm^{-1} was caused by the aromatic ring or C=C stretching vibration, suggesting the formation of carbonyl-containing groups and the carbonization of *Cyperus alternifolius* biomass [52]. The peak at 1,120 cm^{-1} is assigned to the C–C and C–O bond vibrations in acids, alcohols, phenols, ethers, and esters [53]. The light stretching at 840 cm^{-1} might be due to –OH bending, and the band located at 480 cm^{-1} is characteristic of Fe–O [54], indicating that iron is immobilized onto the biochars by chemical bonding. A new band was observed around 1,400 cm^{-1} on FeBC800, which might be due to O–H deformation vibration from carboxylic groups [55].

Fig. 3. SEMs of FeBC pyrolyzed at 400°C (a), 600°C (b), and 800°C (c).

Table 1
Characterization of Fe-impregnated biochars from *Cyperus alternifolius* pyrolyzed at 400°C, 600°C, and 800°C

Samples	S_{BET} ($m^2 g^{-1}$)	S_{mic} ($m^2 g^{-1}$)	%	S_{ext} ($m^2 g^{-1}$)	%	V_{tot} ($m^3 g^{-1}$)	V_{mic} ($m^3 g^{-1}$)	%	d_p (nm)
FeBC400	46.49	39.77	85.54	6.72	14.46	0.039	0.020	51.28	3.34
FeBC600	270.89	227.41	83.94	43.48	16.06	0.18	0.12	66.67	2.66
FeBC800	429.72	352.30	81.98	77.42	18.02	0.30	0.18	60.00	2.82

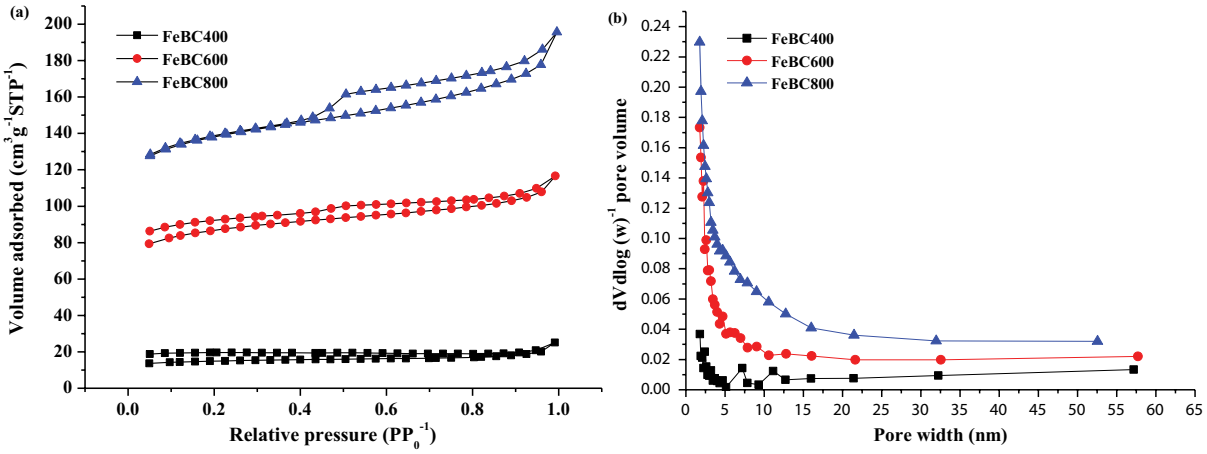

Fig. 4. N_2 adsorption/desorption isotherms (a) and pore size distributions (b) of FeBC pyrolyzed at 400°C, 600°C, and 800°C.

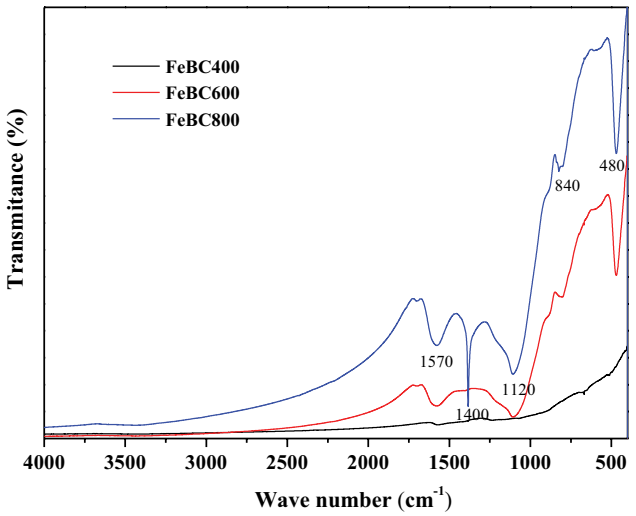

Fig. 5. FTIR spectra of FeBC pyrolyzed at 400°C, 600°C, and 800°C.

3.4. Effects of pH and adsorbent dosage on fluoride removal

The pH of a solution is an important factor for adsorption because it influences the surface charge of the adsorbent and degree of ionization of adsorbate. FeBC600 was selected for further study because it possessed an adsorption capacity for fluoride similar to that of FeBC800. As shown in Fig. 6, removal of fluoride by FeBC600 decreased slightly with an increasing pH in the range of 2.0–10.0. Similar behavior with variation in solution pH has been reported in the adsorption of fluoride by other adsorbents [56,57]. Gago et al. [58] found the total F/free F ratio in the equilibrium solution correlated negatively with soil pH in water. More than 90% removal of fluoride was achieved for all the solution pH range studied, indicating FeBC600 could be used as a convenient adsorbent for fluoride removal without pH adjustment. The maximum value of adsorption was observed at pH 2–3, which was in agreement with the maximum value of pH 3 reported in another study using granular activated carbon coated with manganese oxide [59]. This suggests at low pH, Fe-impregnated hydroxyl groups (Fe–OH) on the biochar are protonated and positively charged, which enhances the adsorption capacity due to electrostatic forces of attraction.

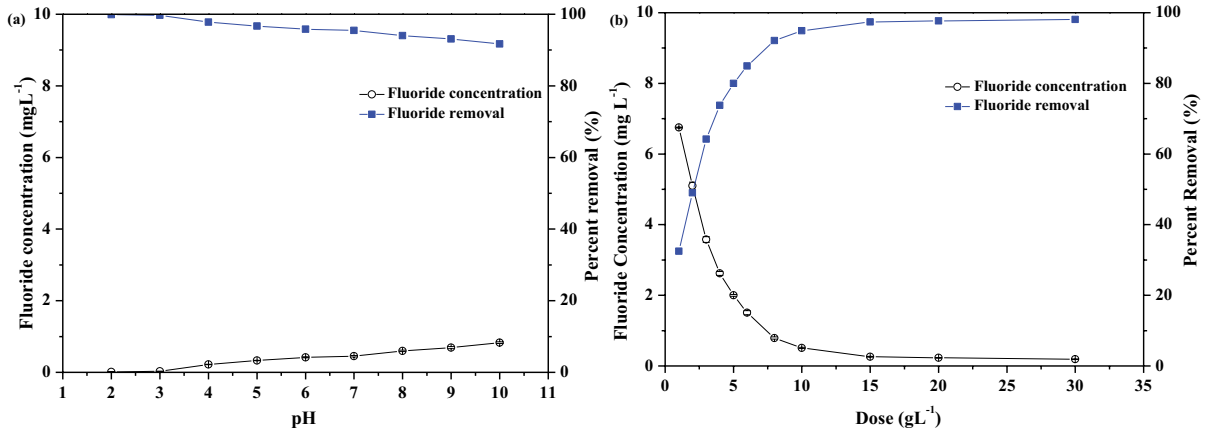

Fig. 6. Effect of initial pH (a) and adsorbent dosage (b) on fluoride removal by FeBC pyrolyzed at 600°C.

Fluoride removal declined under basic conditions possibly due to the competition of hydroxide and fluoride for active sites and increased electrostatic repulsive forces between deprotonated biochar surfaces and the negatively charged fluoride ions [60]. However, fluoride removal was maintained above 90%, indicating that the electrostatic mechanism was not the only mechanism. Other interactions such as hydrogen bonding might be involved as well [56].

The effect of adsorbent on fluoride removal was investigated by varying the adsorbent dosage from 0.1 to 3.0 g in a 10 mg L^{-1} concentration of fluoride solution. It was evident from Fig. 6 that the percentage of fluoride removal increased from 32.5% to 97.4% with an increase of adsorbent dosage from 0.1 to 1.5 g and then remained fairly constant increasing adsorbent dosage, which was higher than the porous starch-Fe and porous starch-La for fluoride concentration of 10 mg L^{-1} [60]. This can be mostly attributed to the increased availability of more active sites with increasing adsorbent dosage. Since the remaining fluoride ion concentration is limited, further increase of adsorbent dose could not promote the further removal of fluoride significantly.

3.5. Adsorption kinetics

In order to more effectively understand the adsorption process, the data obtained were test fitted with pseudo-first-order, pseudo-second-order, and intraparticle diffusion kinetic models. The resultant parameters from these models are shown in Table 2. As seen, the pseudo-second-order kinetic model fitted the data better than the pseudo-first-order model for the entire adsorption range. Correlation coefficients of this pseudo-second-order model were 0.9992 for 10 mg L^{-1} and 0.9966 for 30 mg L^{-1}, larger than those of the pseudo-first-order model. The calculated values of q_e (mg g^{-1}) for fluoride concentrations (mg L^{-1}) of 10 and 30 were 0.988 and 4.99, respectively, indicating a very strong agreement with the experimental values. The removal capacity was much higher than phosphoric acid-modified Mongolian scotch pine tree sawdust char (MMSC) [31], however, lower than Ti (IV)-modified biochar [61]. The pseudo-second-order rate constant (g mg^{-1} min^{-1}) decreased from 0.235 to 0.0238 as the initial fluoride concentration (mg L^{-1}) increased from 10 to 30, suggesting that it would take more time to attain equilibrium at higher initial fluoride concentrations.

The intraparticle diffusion model can be used to identify an adsorption mechanism and to predict the rate-controlling step, wherein the *C* value is related to the boundary layer [34]. If the regression plot of q_t vs. $t^{1/2}$ is linear and passes through the origin, intraparticle diffusion is considered as the rate-controlling step for the adsorption process under study. It can be observed from Fig. 7 that the curves of the two concentrations can each be divided into three portions, and both of the first linear sections do not pass through the origin, which implies that intraparticle diffusion is not the only rate-controlling step, with some other mechanism(s) also possibly controlling the adsorption rate [34]. As shown, k_p decreased and *C* increased with time during the adsorption process. This phenomenon could be interpreted as follows. At the beginning of adsorption, large amounts of active adsorption sites are available on the adsorbent surface, consequently initial adsorption is fast. With the gradual saturation of adsorption sites on the adsorbent surface as well as decreasing fluoride concentration gradient

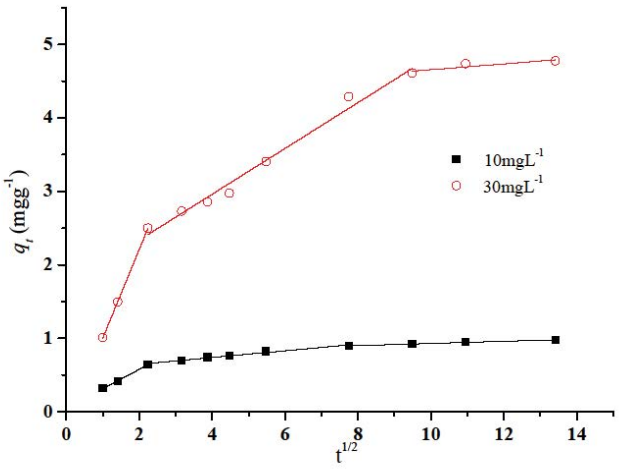

Fig. 7. Intraparticle diffusion model for adsorption of fluoride onto FeBC pyrolyzed at 600°C.

Table 2
Kinetic model parameters for the pseudo-first-order, pseudo-second-order, and intraparticle diffusion models

C_0 (mg L^{-1})	Pseudo-first-order kinetics $\log(q_e - q_t) = \log q_e - \frac{k_1}{2.303} \times t$		Pseudo-second-order kinetics $\frac{t}{q_t} = \frac{1}{k_2 \times q_e^2} + \frac{t}{q_e}$			Intraparticle diffusion $q_t = k_p t^{1/2} + C$		
	k_1 (min^{-1})	R^2	k_2 (g mg^{-1} min^{-1})	q_e	R^2	k_p (mg g^{-1} $min^{-1/2}$)	C (mg g^{-1})	R^2
10	0.0237	0.9305	0.235	0.988	0.9992	0.259	0.0588	0.9937
						0.0461	0.555	0.9664
						0.0144	0.787	0.9839
30	0.0355	0.9887	0.0238	4.99	0.9966	1.21	0.204	0.9999
						0.312	1.71	0.9815
						0.0393	4.26	0.6461

Table 3
Langmuir and Freundlich isotherm parameters for the adsorption of fluoride by FeBC

T (K)	Freundlich equation			Langmuir equation		
	K_F (mg g^{-1} (L mg)$^{-1/n}$)	n^{-1}	R^2	K_L (L mg^{-1})	q_{max} (mg g^{-1})	R^2
293	3.895	0.354	0.9627	0.726	13.624	0.9963
303	4.556	0.349	0.9503	1.170	14.144	0.9985
313	5.434	0.321	0.9534	1.704	14.706	0.9988

near the surface, adsorption becomes less efficient. Also shown in Fig. 7, in the second linear sections of the respective curves, the k_p value for 30 mg L^{-1} was larger than that for 10 mg L^{-1}, indicating the electrostatic repulsion from the fluoride adsorbed on the adsorbent may further hinder the adsorption process as well.

3.6. Adsorption isotherms

Langmuir and Freundlich isotherms [34] were employed to describe the adsorption equilibrium. The calculated isotherm parameters under temperatures of 293, 303, and 313 K are given in Table 3. The equilibrium data fitted well to the two models with R^2 values greater than 0.9500. The maximum adsorption capacity values were 13.624, 14.144, and 14.706 mg g^{-1} under temperatures of 293, 303, and 313 K, respectively, which were in accordance with the actual calculated values. The K_L value increased with the temperature, indicating the increase in temperature may favor the adsorption process. The values of n^{-1} were 0.354, 0.343, and 0.321, respectively, in the range of 0.0–1.0, indicating the adsorption process was favorable.

3.7. Fluoride removal in artificial floating beds with FBC as substrates

All *Cyperus alternifolius* plants grew well, and no obvious toxicity symptoms were observed either in the experimental or control groups. There were no significant differences between experimental treatment plants and control plants in their growth performance during the entire period of the present study. It was found that after 10 d, the average fluoride concentration of the experimental groups was 0.92 mg L^{-1}, thus satisfying the national Class V standard for surface water environmental quality. The fluoride removal of the experimental group was determined to be 46.8% higher than that of control group, with an average fluoride concentration of 3.26 mg L^{-1}. These results strongly suggest that *Cyperus alternifolius* with FBC as substrate might be a feasible alternative for the removal of fluoride of polluted waters. However, elucidating the complex mechanisms involved in the process needs further investigation.

3.8. Desorption and regeneration of FeBC

Seven consecutive adsorption-desorption cycles were performed to study the regeneration and recyclability of FeBC. After seven cycles, the fluoride removal was still higher than 99.0% when the initial fluoride concentration was 10 mg L^{-1}. Therefore, FeBC was suitable for regeneration and could be applied in the fluoride removal.

4. Conclusions

The study confirmed that FeBC prepared from harvested *Cyperus alternifolius* was a good sorbent for removing fluoride. Fluoride removal kept above 90% in the pH over a range of 2.0–10.0. The pseudo-second-order kinetic model provided the best correlation of the experimental data. The equilibrium adsorption data fitted well to Langmuir and Freundlich isotherm models but gave a better fit to the Langmuir model. Fluoride concentration declined from 5 to 0.92 mg L^{-1} in the artificial floating beds with FeBC-rooted *Cyperus alternifolius* in 10 d, satisfying the Class III standard for surface water environmental quality. Besides, the FeBC could be regenerated and reused for several times. Conclusively, the FeBC may be a promising candidate for the removal of fluoride from waters, and the application as substrate for artificial floating beds might be a feasible alternative.

Acknowledgments

This work was supported by the Science and Technology Program of Wenzhou, China (No. S20150006; Z20160011).

References

[1] A. Ramdani, S. Taleb, A. Benghalem, N. Ghaffour, Removal of excess fluoride ions from Saharan brackish water by adsorption on natural materials, Desalination, 250 (2010) 408–413.
[2] V.K. Gupta, I. Ali, Environmental Water: Advances In Treatment, Remediation and Recycling, Elsevier, The Netherlands, 2012.
[3] T. Rafique, S. Naseem, T.H. Usmani, E. Bashir, F.A. Khan, M.I. Bhanger, Geochemical factors controlling the occurrence of high fluoride groundwater in the Nagar Parkar area, Sindh, Pakistan, J. Hazard. Mater., 171 (2009) 424–430.
[4] K. Brindha, R. Rajesh, R. Murugan, L. Elango, Fluoride contamination in groundwater in parts of Nalgonda district, Andhra Pradesh, Environ. Monit. Assess., 172 (2011) 481–492.
[5] V. Tomar, D. Kumar, A critical study on efficiency of different materials for fluoride removal from aqueous media, Chem. Cent. J., 7 (2013) 1–51.
[6] S. Karmakar, J. Mukherjee, S. Mukherjee, Removal of fluoride contamination in water by three aquatic plants, Int. J. Phytorem., 18 (2015) 222–227.
[7] S. Sinha, R. Saxena, S. Singh, Fluoride removal from water by *Hydrilla verticillata* (l.f.) royle and its toxic effects, Bull. Environ. Contam. Toxicol., 65 (2000) 683–690.
[8] M. Baunthiyal, S. Ranghar, Accumulation of fluoride by plants: potential for phytoremediation, Clean Soil Air Water, 43 (2015) 127–132.
[9] P. Pinskwar, M. Jezierska-Madziar, H. Goldyn, E. Arczynska-Chudy, J. Golski, Fluorine content of two submerged plant

species in four Warta River oxbow lake reservoir near Poznan, Poland, Fluoride, 39 (2006) 310–312.
[10] M. Jezierska-Madziar, P. Pinkskwar, Fluoride in common reeds (*Phragmites australis*) sampled from the old Warta reservoirs near Lubon and Radzewice, Poland, Fluoride, 36 (2003) 21–24.
[11] E.I. Reardon, Y.X. Wang, A limestone reactor for fluoride removal from wastewaters, Environ. Sci. Technol., 34 (2000) 3247–3253.
[12] I. Ali, Z.A. ALOthman, M.M. Sanagi, Green synthesis of iron nan-impregnated adsorbent for fast removal of fluoride from water, J. Mol. Liq., 211 (2015) 457–465.
[13] L. Gomez-Hortigueela, A.B. Pinar, J. Perez-Pariente, T. Sani, Y. Chebude, I. Diaz, Ion-exchange in natural zeolite stilbite and significance in defluoridation ability, Microporous Mesoporous Mater., 193 (2014) 93–102.
[14] W. Gong, J. Qu, R. Liu, H. Lan, Effect of aluminum fluoride complexation on fluoride removal by coagulation, Colloids Surf., A, 395 (2012) 88–93.
[15] P.I. Ndiaye, P. Moulin, L. Dominguez, J.C. Millet, F. Charbit, Removal of fluoride from electronic industrial effluent by RO membrane separation, Desalination, 173 (2005) 25–32.
[16] M.H. Dehghani, D. Sanaei, I. Ali, A. Bhatnagar, Removal of chromium (VI) from aqueous solution using treated waste newspaper as a low-cost adsorbent: kinetic modeling and isotherm studies, J. Mol. Liq., 215 (2016) 671–679.
[17] I. Ali, Z.A. AL-Othman, O.M.L. Alharbi, Uptake of pantoprazole drug residue from water using novel synthesized composite iron nano adsorbent, J. Mol. Liq., 2016 (218) 465–472.
[18] I. Ali, Z.A. AL-Othman, A. Alwarthan, Green synthesis of functionalized iron nanoparticles and molecular liquid phase adsorption of ametryn from water, J. Mol. Liq., 221 (2016) 1168–1174.
[19] I. Ali, Z.A. Al-Othman, A. Alwarthan, M. Asim, T.A. Khan, Removal of arsenic species from water by batch and column operations on bagasse fly ash, Environ. Sci. Pollut. Res., 21 (2014) 3218–3229.
[20] I. Ali, Z.A. AL-Othman, A. Alwarthan, Synthesis of composite iron nano adsorbent and removal of ibuprofen drug residue from water, J. Mol. Liq., 219 (2016) 858–864.
[21] K. Biswas, S.K. Saha, U.C. Ghosh, Adsorption of fluoride from aqueous solution by a synthetic iron(III)-aluminum(III) mixed oxide, Ind. Eng. Chem. Res., 46 (2007) 5346–5356.
[22] E.A. Burakova, T.P. Dyachkova, A.V. Rukhov, E.N. Tugolukov, E.V. Galunin, A.G. Tkachev, A.A. Basheer, I. Ali, Novel and economic method of carbon nanotubes synthesis on a nickel magnesium oxide catalyst using microwave radiation, J. Mol. Liq., 253 (2018) 340–346.
[23] I. Ali, O.M.L. Alharbi, Z.A. Alothman, A.Y. Badjah, A. Alwarthan, A.A. Basheer, Artificial neural network modelling of amido black dye sorption on iron composite nano material: kinetics and thermodynamics studies, J. Mol. Liq., 250 (2018) 1–8.
[24] I. Ali, Z.A. Alothman, A. Alwarthan, Uptake of propranolol on ionic liquid iron nanocomposite adsorbent: kinetic, thermodynamics and mechanism of adsorption, J. Mol. Liq., 236 (2017) 205–213.
[25] I. Ali, Z.A. AL-Othman, A. Alwarthan, Molecular uptake of congo red dye from water on iron composite nano particles, J. Mol. Liq., 224 (2016) 171–176.
[26] I. Ali, Z.A. AL-Othman, A. Alwarthan, Removal of secbumeton herbicide from water on composite nanoadsorbent, Desal. Wat. Treat., 57 (2016) 10409–10421.
[27] I. Ali, Z.A. AL-Othman, A. Alwarthan, Supra molecular mechanism of the removal of 17-β-estradiol endocrine disturbing pollutant from water on functionalized iron nanoparticles, J. Mol. Liq., 441 (2017) 123–129.
[28] H. Li, X. Dong, E.B. da Silva, L.M. de Oliveria, Y. Chen, L.Q. Ma, Mechanisms of metal sorption by biochars: Biochar characteristics and modifications, Chemosphere, 178 (2017) 466–478.
[29] M. Ahmad, A.U. Rajapaksha, J.E. Lim, M. Zhang, N. Bolan, D. Mohan, M. Vithanage, S.S. Lee, Y.S. Ok, Biochar as a sorbent for contaminant management in soil and water: a review, Chemosphere, 99 (2014) 19–33.
[30] E. Antunes, J. Schumann, G. Brodie, M.V. Jacob, P.A. Schneider, Biochar produced from biosolids using a sing-mode microwave: characterization and its potential for phosphorus removal, J. Environ. Manage., 196 (2017) 119–126.
[31] X. Guan, J. Zhou, N. Ma, X. Chen, J. Gao, R. Zhang, Studies on modified conditions of biochar and the mechanism for fluoride removal, Desal. Wat. Treat., 55 (2015) 440–447.
[32] L. Cui, Y. Quyang, Y. Chen, X. Zhu, W. Zhu, Removal of total nitrogen by *Cyperus alternifolius* from wastewaters in simulated vertical-flow constructed wetlands, Ecol. Eng., 35 (2009) 1271–1274.
[33] S. Thongtha, P. Teamkao, N. Boonapatcharoen, S. Tripetchkul, S. Techkarnjararuk, P. Thiravetyan, Phosphorus removal from domestic wastewater by Nelumbo *nucifera Gaertn*. and *Cyperus alternifolius* L., J. Environ. Manage., 137 (2014) 54–60.
[34] S.Y. Chu, J.B. Xiao, G.M. Tian, M.H. Wong, Preparation and characterization of activated carbon from aquatic macrophyte debris and its ability to adsorb anthraquinone dyes, J. Ind. Eng. Chem., 20 (2014) 3461–3455.
[35] H. Brix, Do macrophytes play a role in constructed treatment wetlands?, Water Sci. Technol., 35 (1997) 11–17.
[36] S. Ohga, D.J. Royse, Cultivation of *Pleurotus eryngii* on umbrella plant (*Cyperus alternifolius*) substrate, J. Wood Sci., 50 (2004) 466–469.
[37] L.P. Lingamdinne, J.K. Yang, Y.Y. Chang, J.R. Koduru, Low-cost magnetized *Lonicera japonica* flower biomass for the sorption removal of heavy metals, Hydrometallurgy, 165 (2016) 81–89.
[38] L. Liu, J. Sun, C. Cai, S. Wang, H. Pei, J. Zhang, Corn stover pretreatment by inorganic salts and its effects on hemicellulose and cellulose degradation, Bioresour. Technol., 100 (2009) 5856–5871.
[39] K. Fu, Q. Yue, B. Gao, Y. Sun, Y. Wang, Q. Li, P. Zhao, Physicochemical and adsorptive properties of activated carbons from *Arundo donax* Linn utilizing different iron salts as activating agent, J. Taiwan Inst. Chem. Eng., 45 (2014) 3007–3015.
[40] X.Q. Wang, P. Wang, P. Ning, Y.X. Ma, F. Wang, X.L. Guo, Y. Lan, Adsorption of gaseous elemental mercury with activated carbon impregnated with ferric chloride, RSC Adv., 5 (2015) 24899–24907.
[41] K. Raveendran, A. Ganesh, Adsorption characteristics and pore-development of biomass-pyrolysis char, Fuel, 77 (1998) 769–781.
[42] B. Chen, Z. Chen, S. Lv, A novel magnetic biochar efficiently sorbs organic pollutants and phosphate, Bioresour. Technol., 102 (2011) 716–723.
[43] H. Liu, W. Liu, J. Zhang, C. Zhang, L. Ren, Y. Li, Removal of cephalexin from aqueous solutions by original and Cu(II)/Fe(III) impregnated activated carbons developed from lotus stalks: kinetics and equilibrium studies, J. Hazard. Mater., 185 (2011) 1528–1535.
[44] L. Xiao, E. Bi, B. Du, X. Zhao, C. Xing, Surface characterization of maize-straw-derived biochars and their sorption performance for MTBE and benzene, Environ. Earth Sci., 71 (2014) 5195–5205.
[45] B. Chen, Z. Chen, Sorption of naphthalene and 1-naphthol by biochars of orange peels with different pyrolytic temperatures, Chemosphere, 76 (2009) 127–133.
[46] G.N. Kasozi, A.R. Zimmerman, P. Nkedi-Kizza, B. Gao, Catechol and humic acid sorption onto a range of laboratory-produced black carbons (biochars), Environ. Sci. Technol., 44 (2010) 6189–6195.
[47] M. Uchimiya, L.H. Wartelle, T. Klasson, C.A. Fortier, I.M. Lima, Influence of pyrolysis temperature on biochar property and function as a heavy metal sorbent in soil, J. Agric. Food. Chem., 59 (2011) 2501–2510.
[48] R.A. Brown, A.K. Kercher, T.H. Nguyen, D.C. Nagle, W.P. Ball, Production and characterization of synthetic wood chars for use as surrogates for natural sorbents, Org. Geochem., 37 (2006) 321–333.
[49] H. Yang, R. Yan, H. Chen, D.H. Lee, C. Zheng, Characteristics of hemicellulose, cellulose and lignin pyrolysis, Fuel, 86 (2007) 1781–1788.

[50] T. Garcia, R. Murillo, D. Cazorla-Amoros, A.M. Mastral, A. Linares-Solano, Role of the activated carbon surface chemistry in the adsorption of phenanthrene, Carbon, 42 (2004) 1683–1689.
[51] P.R. Bonelli, P.A. Della Rocca, E.G. Cerrella, A.L. Cukierman, Effect of pyrolysis temperature on composition, surface properties and thermal degradation rates of Brazil Nut shell, Bioresour. Technol., 76 (2001) 15–22.
[52] A. Rathinam, J.R. Rao, B.U. Nair, Adsorption of phenol onto activated carbon from seaweed: determination of the optimal experimental parameters using factorial design, J. Taiwan Inst. Chem. Eng., 42 (2011) 952–956.
[53] H.P. Boehm, Surface oxides on carbon and their analysis: a critical assessment, Carbon, 40 (2002) 145–149.
[54] A.O.A. Tuna, E. Ozdemir, E.B. Simsek, U. Beker, Optimization of process parameters for removal of arsenic using activated carbon-based iron-containing adsorbents by response surface methodology, Water Air Soil Pollut., 224 (2013) 1685.
[55] H. Liu, P. Dai, J. Zhang, C. Zhang, N. Bao, C. Cheng, L. Ren, Preparation and evaluation of activated carbons from lotus stalk with trimethyl phosphate and tributyl phosphate activation for lead removal, Chem. Eng. J., 228 (2013) 425–434.
[56] A. Sivasamy, K.P. Singh, D. Mohan, M. Maruthamuthu, Studies on defluoridation of water by coal-based sorbents, J. Chem. Technol. Biotechnol., 76 (2001) 717–722.
[57] M. Streat, K. Hellgardt, N.L.R. Newton, Hydrous ferric oxide as an adsorbent in water treatment: part 3: batch and mini-column adsorption of arsenic, phosphorus, fluorine and cadmium ions, Process Saf. Environ. Prot., 86 (2008) 21–30.
[58] C. Gago, A. Romar, M.L. Fernandez-Marcos, E. Alvarez, Fluorine sorption by soils developed from various parent materials in Galicia (NW Spain), J. Colloid Interface Sci., 374 (2012) 232–236.
[59] Y. Ma, S.G. Wang, M. Fan, W.X. Gong, B.Y. Gao, Characteristics and defluoridation performance of granular activated carbons coated with manganese oxides, J. Hazard. Mater., 168 (2009) 1140–1146.
[60] L. Xu, G. Chen, C. Peng, H. Qiao, F. Ke, R. Hou, D. Li, H. Cai, X. Wan, Adsorptive removal of fluoride from drinking water using porous starch loaded with common metal ions, Carbohydr. Polym., 160 (2017) 82–89.
[61] B.R. Vilakati, V. Sivasankar, E.N. Nxumalo, B.B. Mamba, K. Omine, T.A.M. Msagati, Fluoride removal studies using virgin and Ti (IV)-modified Musa paradisiaca (plantain pseudo-stem) carbons, Environ. Sci. Pollut. Res., (2018). https://doi.org/10.1007/s11356-018-2691-x.